Finite Element analysis of CFRP laminates subjected to compression after edge impact

Benjamin Ostré, Christophe Bouvet, Clément Minot, Jacky Aboissière

Finite element analysis of CFRP laminates subjected to compression after edge impact

Benjamin Ostré [a], Christophe Bouvet [a,*], Clément Minot [b], Jacky Aboissière [b]

[a] Université de Toulouse, ICA, ISAE-Supaéro, 10 Avenue Édouard-Belin, BP 54032, 31055 Toulouse Cedex 4, France
[b] SOGETI High Tech, Aéropark, 3 chemin de Laporte, 31300 Toulouse, France

ABSTRACT

Composite structures are particularly vulnerable to impact which lowers drastically theirs residual strength. In particular, the edge impact on composite stiffener is known as a critical factor on the loss of residual compression strength. Then it is necessary to develop a model able to simulate impact and compression after impact in order to numerically optimize composite structures within impact damage tolerance.

In the present paper, a unique model, based on Discrete Ply Model, allows to simulate edge impact and compression after impact (CAEI) of two stacking sequences highly oriented, representative of a real aeronautical stiffener structure. A relatively good correlation is found between experiment and model regarding the important number of phenomena which is taken into account: permanent indentation after impact, force–displacement impact curve, crack length after impact, delamination after impact, stress-displacement CAEI curve, stress-out-of-plane displacement curve, CAEI final failure. Moreover only 14 parameters are needed to feed this model, and all are obtained using standard tests and have physical relevance. This concept is important because it allows considering running similar tests with other materials without performing complex and special identification tests but only using physical parameters of standard tests. The good results of this approach could allow to define a new design method to improve the edge impact damage tolerance.

1. Introduction

Composites are widely used in the aeronautical field due to their high specific stiffness and strength, corrosion resistance and fatigue performance. Unfortunately, the aeronautical composite structures could be significantly damaged by foreign tools during manufacturing or maintenance operations and the damage occurring might remain undetected by visual inspection [1–3]. Aeronautical industry certification needs the proof of the impact resistance depending upon the impact damage detectability of these structures, which is known as the damage tolerance concept [1–4].

For example free edge composite stringers of an airplane's centre wing box are strongly loaded and are designed to resist to buckling and to keep the structure safe, but if a tool drops on a stringer edge during the plane's maintenance, its residual properties can be drastically reduced [5,6]. Improvement of the edge impact damage tolerance could be achieved by better understanding of the damage scenario of edge impact and compression after edge impact (CAEI) and by developing a finite element model based on this damage scenario. Compression after impact (CAI) is generally the final step to establishing the structure's residual strength for aeronautical certification, because compression is classically the most affected characteristic by impact damage [2].

The current edge impact detectability threshold criterion for aeronautics is driven by the dent depth and the crack length. When the impact indentation is smaller than the barely visible impact damage (BVID) and the crack length less than a given threshold value, the structure has to support the extreme loads to which it may be subjected. However, if the damage is detectable, i.e. when the impact indentation is bigger than the BVID or the crack length higher than a given threshold value, a repair or change of the structure must be considered [7,8].

Many studies have been carried out on composite skin and panel impact issues, both theoretically and experimentally. Impact and CAI damage scenarios are now fairly well developed [9–16]. However, if the focus is shifted from skin to edge, then there seems a lack of knowledge regarding, in particular, the residual strength.

* Corresponding author.
  E-mail address: christophe.bouvet@isae.fr (C. Bouvet).

To the author's knowledge, only a few researches have been conducted in this regard [6,12,13,16,17] which elaborate CAEI mechanisms and show that composite structures are particularly vulnerable to edge impact. This remark is already true for modelling; only a few studies deal with modelling of edge impact and CAEI [12,17,18].

Nevertheless, in order to numerically design and optimize a composite within the impact damage tolerance, it is necessary to simulate the edge impact, in particular the impact damage and the detectability data, as well as the CAI, in particular the effect of the impact on the residual strength. Moreover the consecutive modelling of impact and CAI leads to addition of the discrepancies from both models. In fact the complete numerical simulation of impact damage and CAI is still a challenge and is the subject of much research [15,17–23].

Then the first step to achieve, in order to model the edge impact damage tolerance, is to simulate the edge impact. This modelling is not the subject of the present paper but is that of a previous publication [21]. Yet it is important to understand edge impact modelling in order to understand the CAEI. It seems one of the key points of the edge impact modelling is the wedge, or swelling, effect [24]. In order to simulate the swelling effect and then to simulate the delaminations obtained during impact, it is necessary to take into account the expansion of the plies in the transverse, and in the out-of-plane, directions when it is crushed in the loading direction.

The second step to achieve, in order to model the edge impact damage tolerance, is to simulate the CAEI. This is of course the subject of this paper. In the literature, only a few papers put forward a model able to simulate with the same model, the impact and the CAI [15,17,19,20]. In the case of impact on flat panel, the key point of CAI modelling is the effect of the impact damage on the residual strength, and in particular how this impact damage evolves during the CAI test. For some authors, the buckling of the plies, delaminated during the impact, is responsible for the final failure and then drives the residual strength of the structure [1]. At the same time, a strain (or stress) concentration is observed at the boundary of the damage area, especially on the impacted side. When the strain concentration reaches the compression failure strain, a crack propagates, leading to the structure's final failure [15–18]. Of course these 2 phenomena, the buckling of delaminated interfaces and the propagation of a compressive fibre crack, should be linked and feeding each other. But it is important to understand these phenomena in order to be able to simulate the final failure of a CAI test taking into account the physics of damage propagation.

Then the scenario of final failure of CAI being not so clear, it is also the case of the CAEI scenario. Indeed, to the authors' knowledge, there is no model in the literature simulating edge impact and CAEI with the same model. This is also the aim of this article to propose a model able to simulate all the edge impact damage tolerance.

Nevertheless, some models in the literature are able to model the CAEI, and reach to evaluate the failure stress [13,17–19,25–27]. For example, Suemasu et al. [18] use the delaminations obtained experimentally in a finite element of CAEI. They show the buckling of the delaminated plies allows to predict the final failure, and then the residual strength. This result is important because it seems to confirm the major role played by the buckling of delaminated plies on the final failure.

Rhead et al. [12,13] adopted similar approach and show it is possible to predict the final failure of the structure during the CAEI simulating the buckling of the delaminated plies. The out-of-plan swelling, considered as an initial buckling, and the delaminated area, measured by C-SCAN, are considered as initial data and slightly increased to ensure a safety coefficient. Delamination is then determined considering mode I (opening fracture mode) as

the leading mode. The model is in good agreement with experiment and seems to confirm the major role of the local buckling.

Of course, the major drawback of these types of modelling is the need to know the impact damage to simulate the CAEI, and then to be unable to estimate the impact damage tolerance of a composite structure.

Another approach consists in comparing the loss of residual strength obtained after edge impact, to these ones obtained with an open hole. This idea of open hole model is often used for flat panels [27,28,16]. In [28], Ostré et al. used this idea, coupled with a "point stress approach" [29], to evaluate the residual strength after edge impact. The good correlation of this model seems to confirm that propagation of the compression fibre failure plays a major role in the mechanism that drives the laminate residual strength after edge impact.

Then there is a lack of acquaintance in the literature on the CAEI and in particular on the modelling of the CAEI. Moreover the failure scenario of CAEI is not grasped and some work seems needed to highlight the final damage propagation. That is why, in this paper, like the previous authors' edge impact studies [21,30,31], the damage scenario drives the numerical analysis of the CAEI. Especially, the main question is to find how the final failure occurs. That is why we need to define a unique model (edge impact + CAEI) which includes these phenomenon in order to give the right final failure criteria. In addition, the complementarity of the different CAEI experiments carried out with the model developing allows to improve the physical understanding of the phenomenon.

2. Specimen configuration for edge impact and CAEI tests

In this study, all the experiments were carried out with the same laminates than the edge impact analysis [21,28,31]. The stacking sequences are representative of the current industrial needs. The specimen presents the same size as that of a real-life stringer structure, i.e. 150 mm long, 60 mm high specimen with 30 mm free outside boundary conditions (Fig. 1).

T700/M21 UD carbon prepreg was selected, which is a very well-known aircraft material [15], and its properties found from standard tests are listed in Table 1.

Following two different stacking sequences were defined:

- **Stacking A:** [90_2, -45_2, 0_4, 45_2, 0_2]$_s$, 6 mm-thick for 24 plies.
- **Stacking B:** [45_2, 0_2, -45_2, 0_4, 90_2]$_s$, 6 mm-thick for 24 plies.

Firstly, impact tests are performed with a special test set up [31] (Fig. 1a). This set up was designed in order to simulate the same boundary conditions that a classical "stringer + skin" structure, with a simple plane sample, avoiding the complex manufacturing of a stringer.

Secondly, CAEIs were performed with a special test set up [28] (Fig. 1b) designed in order to simulate the same boundary conditions that a classical "stringer + skin" structure. The main goal is to build a guide-rail type connection on the specimen that does not disturb the damage due to the edge impact. This tool is inspired from Boeing's standard BSS 7260 [32,33]. The major difference with the Boeing's standard BSS 7260 [33] is the positioning of two guiding knives (Fig. 1b). These two guiding knives are made of 4 blades (one on each side of the plate) which allow the specimen's translation on the compression direction as a guide rail-type connection.

3. Damage modelling

The model of composite damage used in this study, named "Discrete Ply Model" (DPM) was simulated with Abaqus Explicit
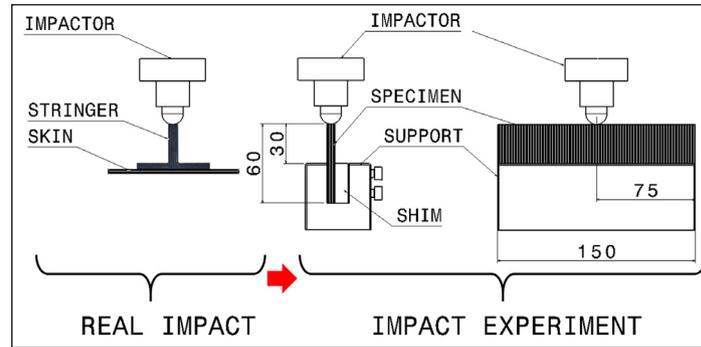
-a-
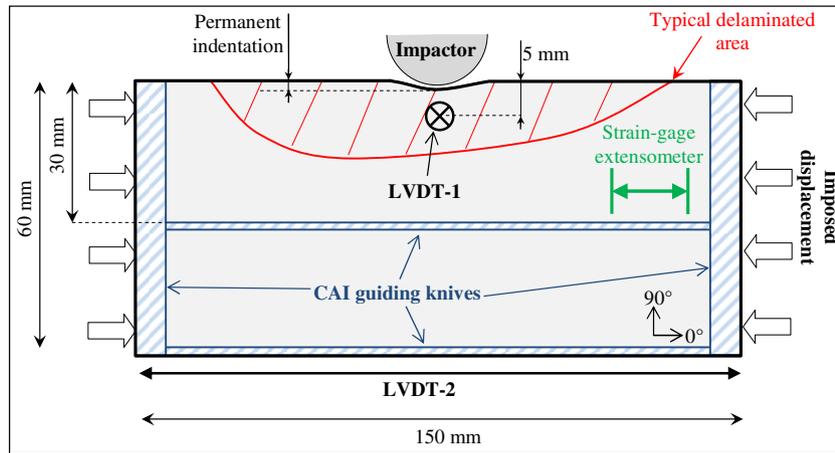
-b-

Fig. 1. Experimental set-up of edge impact (a) and guide-rail type connection realised with guiding knives for CAEI (b).

Table 1
Mechanical material properties of T700/M21 UD for "Discrete Ply Model" (DPM) [15].

| Carbon/epoxy T700/M21 UD properties for DPM		
e	Ply thickness	0.25 mm
E_l^t	Longitudinal tensile Young's modulus	130 GPa
E_l^c	Longitudinal compressive Young's modulus	100 GPa
E_t	Transverse Young's modulus	7.7 GPa
G_{lt}	Shear modulus	4.75 GPa
v_{lt}	Poisson's ratio	0.33
ε_l^t	Longitudinal tensile failure strain	0.016
ε_l^c	Longitudinal compressive failure strain	−0.0125
σ_t^t	Transverse tensile strength	60 MPa
σ_t^c	Transverse compressive strength ($=\sigma_t^{crush}$)	−250 MPa
τ_{lt}	In-plane shear strength	110 MPa
G_I	Interlaminar mode I fracture toughness	0.65 N/mm
G_{II}	Interlaminar mode II fracture toughness	2.08 N/mm
G_I^f	Fibre tensile mode I fracture toughness	130 N/mm
G_I^c	Fibre compressive mode I fracture toughness	40 N/mm
f	Friction coefficient	0.06
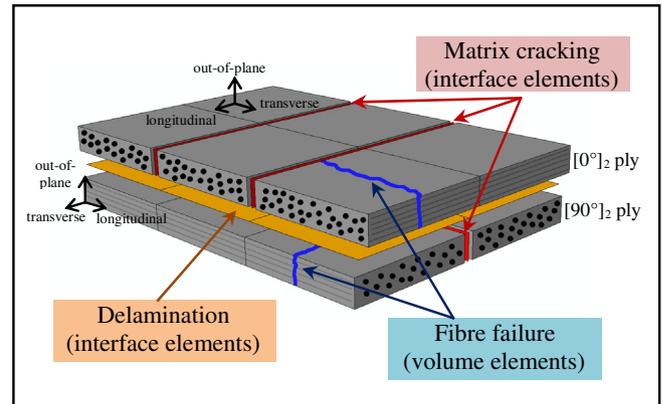
Fig. 2. Modelling of composite damages with the different element types in each oriented ply [15].

(version 6.9) and extensively presented in [4,15,21,30]. Only a brief recall is done in order to better understand the CAEI model and the interested reader can find more details in [4,15,21,30]. The principle is to simulate the major failure modes observed in composite impact tests as follows (Fig. 2):

The delamination is simulated with classical interface elements between two consecutive plies; each ply being modelled with one volume finite element in the thickness. Then the damage in the delamination interface elements is classically driven using fracture mechanics.

The intra-ply matrix cracking is simulated using interface elements normal to the transverse direction. The damage in the matrix cracking interface elements is driven using stress criterion written in the neighbouring volume elements. These interface elements constrain to a complex mesh, but permit to naturally obtain the coupling between intra- and interlaminar damage. This coupling is known as crucial to simulate the complex damage morphology developing in composite structures during impact [23,34]. Moreover the crushing in the transverse direction should be taken into account, in particular during the impact test, for example for the mid-thickness 90° ply of the stacking B aligned with the impact loading direc-
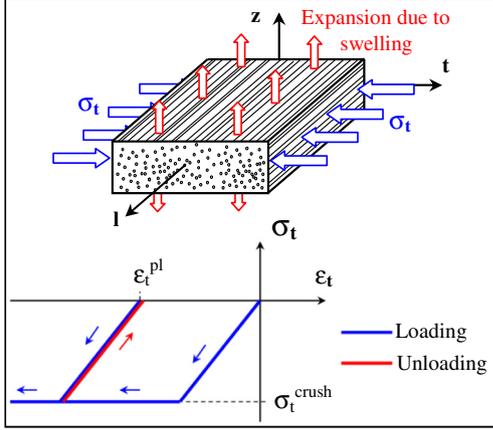
Fig. 3. Crushing principle in the transverse direction.

tion. Thus a plastic behaviour is implemented in the transverse direction [21] and a coupling is introduced with the out-of-plane direction in order to simulate the swelling effect (Fig. 3):

$$\varepsilon_t^{pl} \text{ such as } f_t = |\sigma_t - \sigma_t^{crush}| \leqslant 0 \text{ and } \dot{\varepsilon}_z^{pl} = -\dot{\varepsilon}_t^{pl} \tag{1}$$

where ε_t^{pl} (ε_z^{pl}) is the plastic strain in the transverse (out-of-plane) direction, σ_t the stress in the transverse direction, σ_t^{crush} the crushing stress in the transverse direction, f_t the yield function [35] and the over-dot the time derivative. This equality (in absolute value) of the plastic strains in transverse and out-of-plane directions equates to impose a volume conservation of the ply during crushing. This is a preliminary approach allowing to simulate the swelling effect without adding material parameters. To confirm this swelling effect, the calculation was done without this coupling and the result showed almost no delamination.

Indeed the objective of the DPM is to physically simulate the damage mechanisms of composite with a limited number of parameters. Indeed the material parameters, in composite damage modelling, are often difficult to evaluate and without clear physical signification. In the present approach, only physical parameters are used, which can be evaluated with standard tests (Table 1). This swelling effect is of first importance during the impact test, because it induces the out-of-plane laminate swelling and the delamination propagation.

The fibre failure is simulated using conventional continuum damage mechanics but with original formulation between the integration points of the element to produce a constant energy release rate per unit area (more details can be found in [21]). This approach can be compared to methods based on characteristic element length which makes possible mesh-size independent modelling [36–38]. Moreover, a crushing model is used in order to simulate the crushing developing during impact under the impactor (for example for the mid-thickness 0° ply of the stacking A aligned with the impact loading direction). This crushing process

constrains a communication between elements in the longitudinal direction in order to transmit crushing between consecutive volume elements [21,24,39]. In the same way as Israr et al. [24], when crushing is reached, crushing is transmitted (Fig. 4) to the two neighbouring elements (or with the neighbour element if it is an edge element). Indeed once the crushing process is initiated, the neighbouring elements cannot reach the failure compression stress in the longitudinal direction anymore, nor to dissipate the fracture toughness of compressive fibre failure.

4. Edge impact modelling

In order to help the reader to understand this paper, the authors present the main conclusions of the edge impact model of the stacking sequences A and B study [21]:

From a qualitative and quantitative point of view, edge impact model causes the delamination of all the interfaces as well as the experimental study (Fig. 5). The model seems to restore fibre failure, matrix cracking and delamination during the experiment in an adequate way.

From a quantitative point of view, the force–time curves show a relatively good correlation in terms of total impact time and force drop; the phenomenon is thus well restored in time for the both stacking sequences (Fig. 6). Nevertheless, the model seems to pass in an adequate way from compressive fibre failure to crushing process. This problem could be due to the crushing modelling (Fig. 4).

Projected delaminated area presents a good agreement between experiment and modelling for stacking A, whereas stacking B underestimates this delaminated area by 55% on average. Nevertheless the damage form seems faithfully simulated for the two stackings sequences [21].

Finally, a relatively good experiment/model agreement is revealed concerning the results of the parameters retained by industry (Fig. 7); the maximum crack length on the edge and the permanent indentation. Of course, the higher the impact energy, the longer the crack.

This edge impact model is similar to the DPM on laminate specimen with the addition of new friction and crushing behaviours. The trends are restored overall but obviously there is still some consequent work to be done to better understand the damage scenario and in particular the strain rate effect on the compression and the crushing behaviours. The choice of the proposed approach is to limit as much as possible the number of material parameters and to only introduce parameters with physical signification, which can be evaluated with standard tests. In the present case, 14 parameters are needed: 5 for stiffness, 5 for failure stress or strain and 4 for fracture toughness (Table 1).

Now, this model is applied to the compression after impact test.

5. CAEI modelling

The CAEI model has the same architecture than the edge impact model; new boundary conditions (Fig. 8) are the only modifications
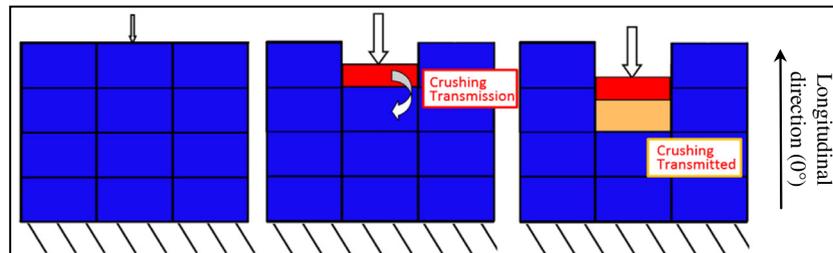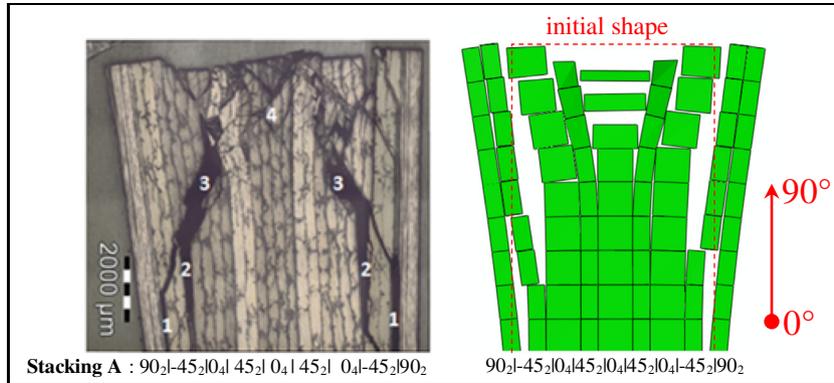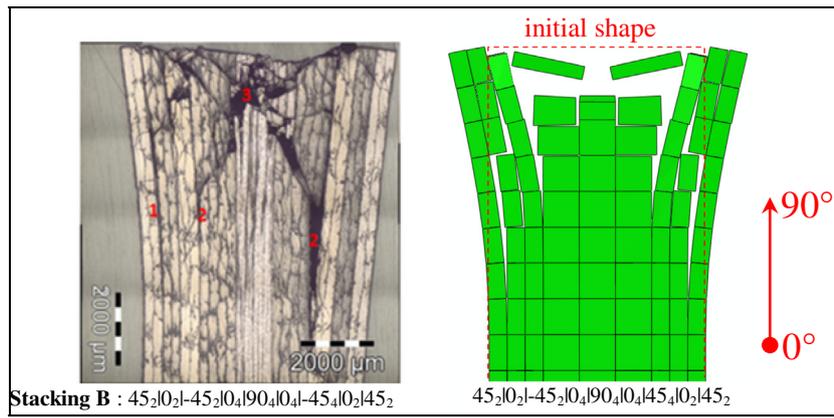

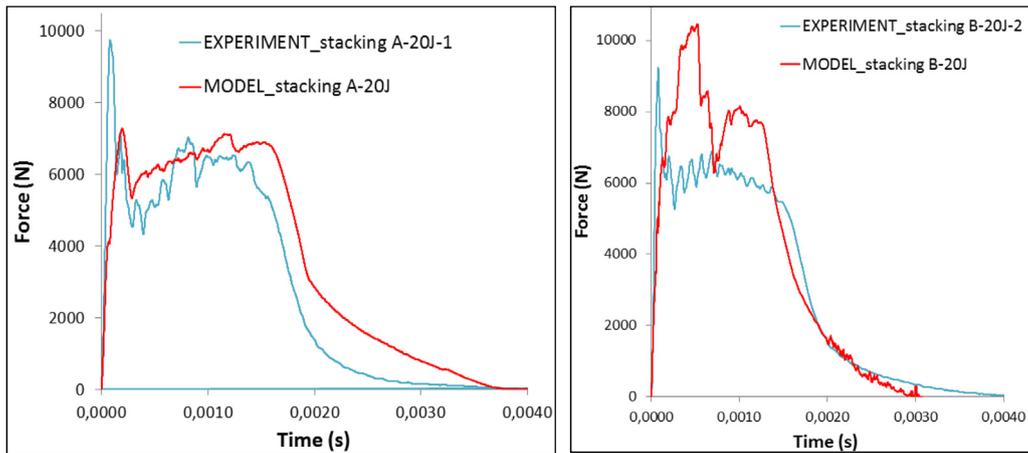**Fig. 4.** Crushing transmission principle.

Fig. 5. Experiment/model comparison of cut sections of stacking A (a) and B (b) impacted at 10 J just under the impactor.

Fig. 6. Experiment/model comparison of the edge impact force/time curves of the stacking A (a) and B (b) impacted 20 J (b).

required in order to add a compressive loading after the edge impact (equivalent to the CAEI experiment exposed in [28]). Of course the modelling is exactly the same for edge impact loading and for CAEI loading. Firstly the impact is simulated until the impactor rebound. This first step lasts typically 5 ms (in fact the time depends on impact energy; more is the impact energy, longer is the impact) (Fig. 14a). Secondly, the structure should be stabi-

lized to avoid oscillations due to impact loading. This stabilization is obtained using successive stops and releases of the velocity of all the points of the structure. This step lasts typically 0.75 ms (this time step is decreased as much as possible to obtain stabilization of oscillations while saving calculation time) (Fig. 14a). At the same time, the boundary conditions of impact are removed and those of compression are introduced. Finally the compressive displacement
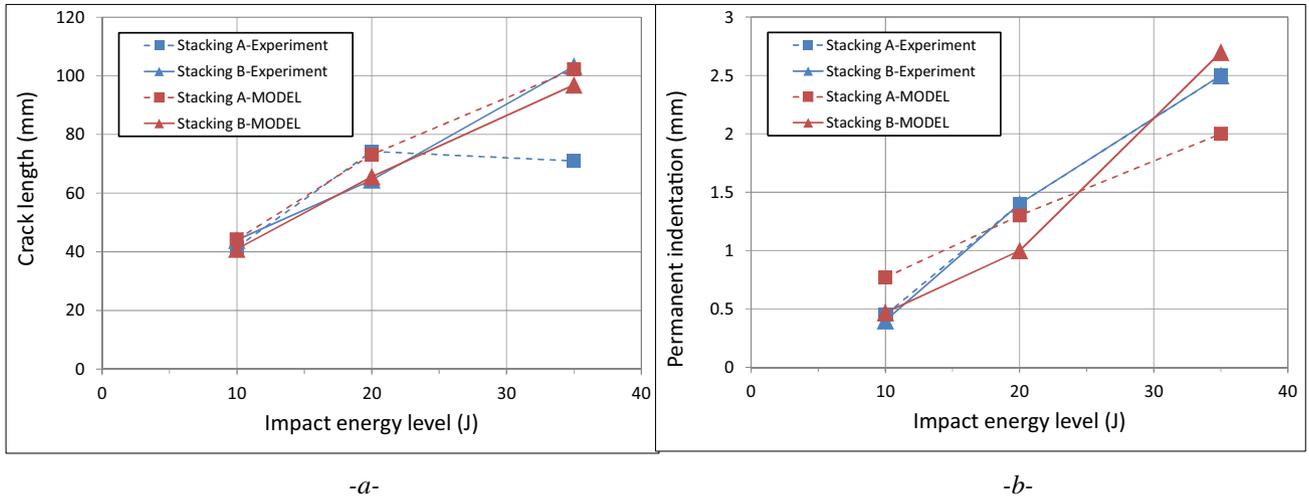
Fig. 7. Experiment/model comparison of maximum crack length (a) and permanent indentation (b) versus impact energy.
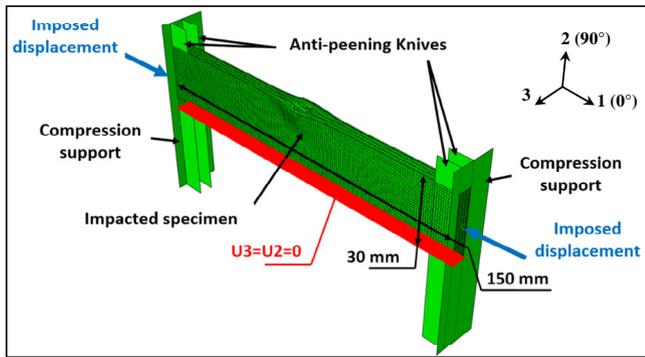

Fig. 8. Model principle of CAEI.

is imposed. During this last step, it is not possible to use the real time of the test, because the compression test is a static test and the modelling is an explicit model. Thus a fictive time is used in order to minimize the test time, and then to save calculation time, and at the same time to be representative of the static compression. This step lasts about 4 ms (even if the final failure could be achieved before the step end) (Fig. 14a). Once this fictive time was chosen, it is necessary to verify that the model was robust to any time change. This work has been done and shows there is no significant difference between steps of 4 ms and steps of 20 ms, confirming the validity of the adopted choice.

Thus, stacking A and B, impacted at 10, 20 and 35 J energy levels, were modelled. The two other stacking sequences tested in the experiment [28] will have to be modelled in the future. In
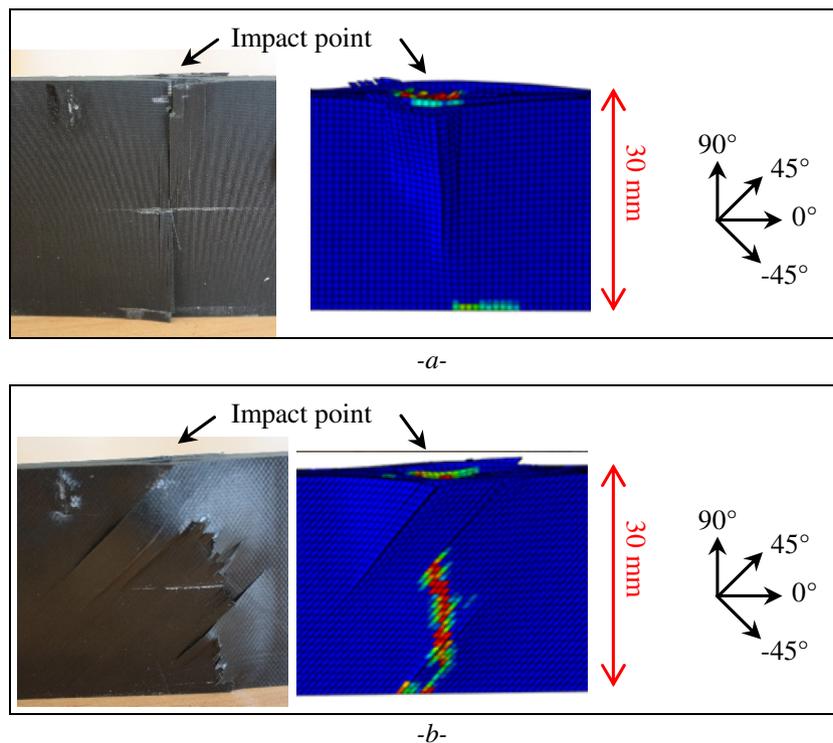

-a-

-b-

Fig. 9. Experiment/model comparison of the CAEI failure, stacking A (a) and stacking B (b).

addition, the choice was made to represent half of the specimen (30 mm large for the model against 60 mm large for the real specimen) to save calculation time. Indeed, the edge impact damage never reaches the boundary conditions. A set of nodes (in red colour in Fig. 8) opposed to the impact is thus defined free to translate in the compression direction (U1), but the transverse (U2) and out-of-plan (U3) displacements are locked to ensure a similar boundary condition to the experiment tool (Fig. 1b). The total compression force F_{real} is then estimated as the sum of the measured force on the model F_{Model} and the half specimen force (not represented) $F_{1/2}$ as follows:

$$F_{real} = F_{Model} + F_{1/2} = F_{Model} + \varepsilon_{av} \cdot E_{av}{}^* S_{1/2}$$
$$= F_{Model} + \frac{d_{imp}}{L} \cdot E_{av}{}^* S_{1/2} \qquad (2)$$

where ε_{av} is the model average compression strain, E_{av} the laminate average stiffness in the compression direction (57 GPa for the stacking A and B), L the specimen length in the 1-direction (L = 150 mm), d_{imp} the imposed displacement and $S_{1/2}$ the not displayed half specimen surface ($S_{1/2}$ = 180 mm^2).

6. Results

The main goal of this study is to test, from a qualitative and quantitative point of view, the DPM used for edge impact simula-

tion [21] under compressive loading (Imposed displacement in the specimen's longitudinal direction) (Fig. 1b).

6.1. Qualitative results

A visual comparison between experiment and model damage picture is carried out. A relatively good correlation is found between experiment and model regarding the specimen's external surface after failure (Fig. 9). This good correlation confirms qualitatively the quality of the damage state obtained after CAEI. The central crack of stacking A is well represented by the model (Fig. 9a). In addition, matrix cracks, buckling and 45° plies failure of stacking B outside surface are relatively realistic (Fig. 9b). The final failure propagation is, for the experiment as for the model, localised at the specimen's centre (normal to the compressive loading) and has its origin at the impact point. The model seems to adequately restore the fibre failure and the matrix cracks of the experiment specimen's outside surface.

6.2. Quantitative results

From a quantitative point of view, the first step to achieve is the analysis of the force-imposed displacement curves (Fig. 10). For both stacking sequences (stacking B is not shown, because results are similar), a progressive force rising is observed, then a maximum force is reached and finally the force drops sharply, both
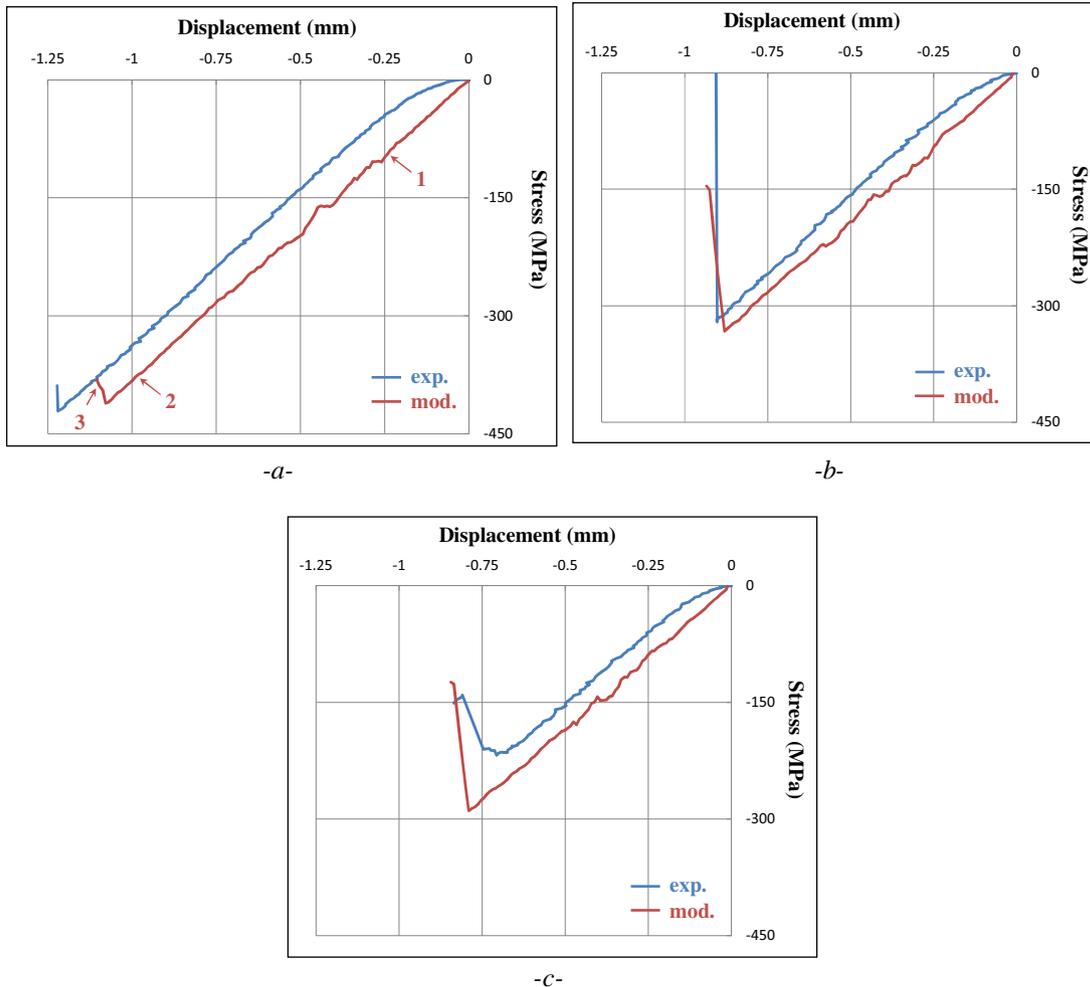

Fig. 10. Experiment/model comparison of the stress-imposed displacement curves; stacking A impacted at 10 J (a), 20 J (b) and 35 J (c).

experimentally and numerically. The correlation is not as good for 35 J tests (for stacking A or B) where some non-linearity is experimentally obtained just before the final failure; which is not numerically obtained.

It can be noticed a non-linear behaviour is observed at the beginning of the experimental tests. This phenomenon is due to the classical problem of sample positioning at the test start and should not be considered for interpretation. Of course this phenomenon is not obtained with modelling. But if the non-linearity is removed from the experimental results in Fig. 10 and an apparent zero used, the results appear to be in good agreement.

On one hand, for stacking sequence A (Fig. 10a and b), the force–displacement curves numerically obtained are in good agreement with the experiments conducted at 10 J and 20 J energy levels. On the other hand, the model does not match very well the experiment impacted at 35 J, and the failure force is overestimated (the result is similar for stacking B). At the same time, the failure numerically obtained is very sharp, contrary to the failure experimentally obtained which is smoother. It is difficult to conclude if the model is too sharp, due to the low number of experiments. Other experiments should be done in order to confirm, or not, the type de failure.

The second step to achieve is the comparison of the curves of stress versus out-of-plane displacement (Fig. 11). The out-of-plane displacement is obtained experimentally using a LVDT sensor (LVDT1 in Fig. 1b) situated about 5 mm under the impact point

on the outside surface. For the 10 J-CAEI, the correlation is relatively good, even if a drop of the out-of-plane displacement is experimentally obtained at about -350 MPa, which is not numerically obtained. Nevertheless, this out-of-plane drop is not obtained with stacking B and other tests are necessary to confirm if this phenomenon is repeated.

It can be noticed from every curves that the model overestimates the out-of-plane displacement. Particularly for the 20 and 35 J-CAEI, the slope at the origin (Fig. 11b and c) is overestimated by the model: the experiment shows a more progressive swelling. In order to illustrate the swelling effect obtained by modelling, Fig. 12 presents the section of the plate in the $(2, 3)$ plane (Fig. 8) just under the impactor. In this figure, the d_{fibre} denotes the fibre damage, which equals 0 if the material is undamaged and 1 if the material is totally damaged (in fact this damage is limited to 0.99 to avoid excessive distortion of elements). The different phases of the calculation can be seen; the shape before impact ($t = 0$ ms), the shape at the maximum deformation during impact ($t = 1.25$ ms), the shape after impact, and stabilization, just before CAEI ($t = 5.75$ ms), the shape during CAEI just before finale failure ($t = 8.5$ ms) and the shape just after final failure ($t = 8.75$ ms). The time correspondence can be found in Fig. 14a (see next paragraph for explanation of Fig. 14). Swelling is very important and particularly during impact and at the end of the CAEI. It can be noticed that the out-of-plane displacement plotted in Fig. 11 does not take into account the swelling obtained after
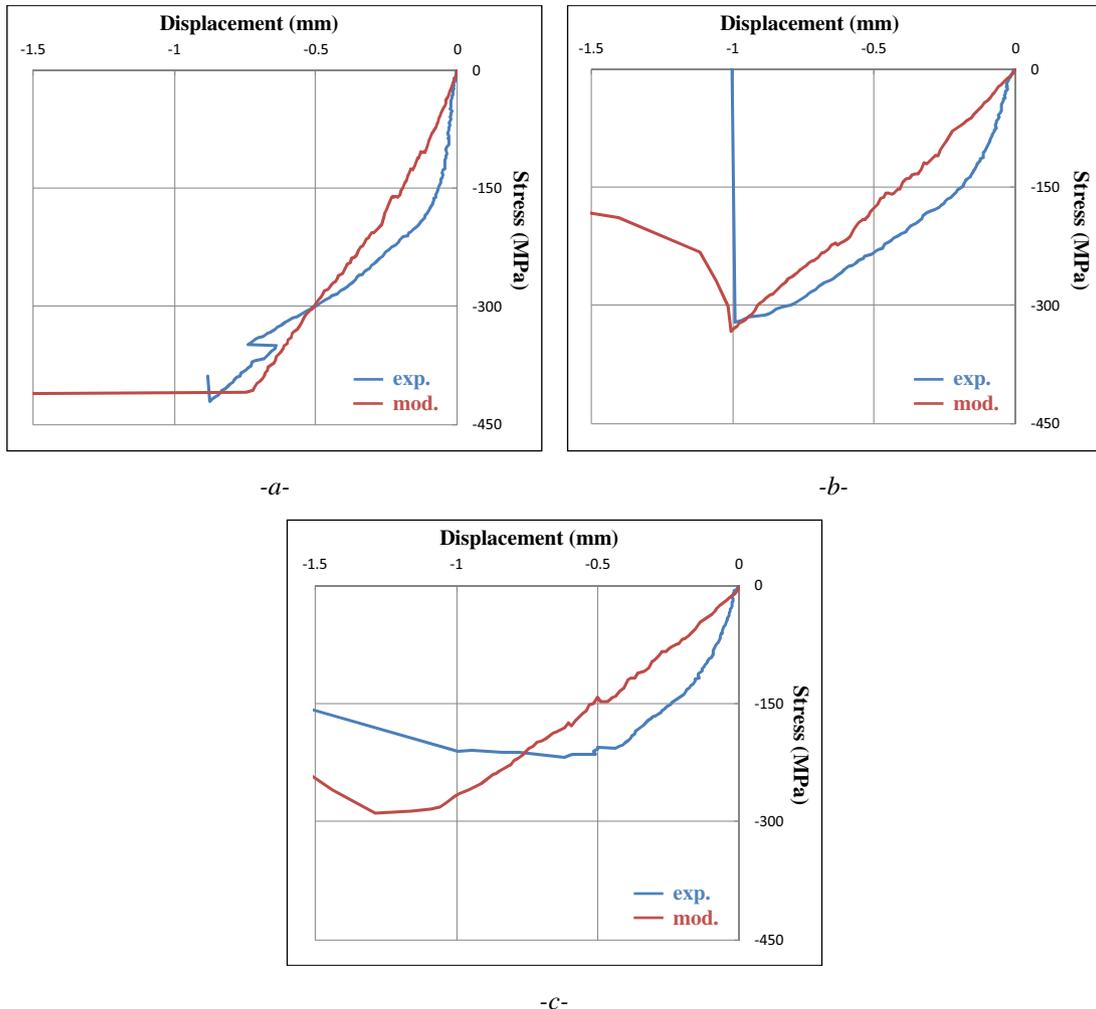

Fig. 11. Experiment/model comparison of the curves of stress versus out-of-plane displacement, stacking A impacted at 10 J (a), 20 J (b) and 35 J (c).
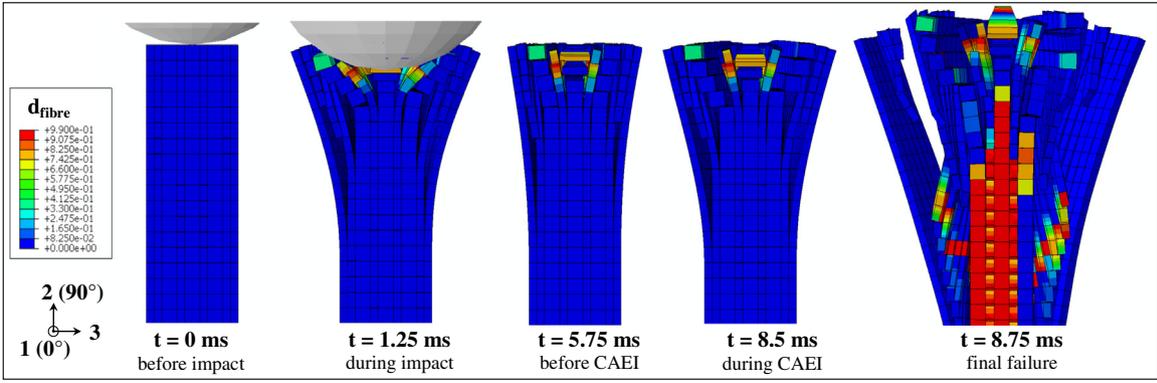
Fig. 12. Section in the (2, 3) plane just under impactor of stacking A impacted at 10 J.

impact and is taken null at the beginning of CAEI, as for experiment. This swelling obtained after impact can be seen in Fig. 5 and is globally overestimated by model. This discrepancy in the edge impact modelling could explain the discrepancy obtained during CAEI (Fig. 11). Some phenomenon could explain this discrepancy, for example the relaxation after impact which is not modelled, or the shape of the debris in the zone just under the impactor obtained after impact (Fig. 5). Nevertheless, the magnitude of swelling and out-of-plane displacement is globally obtained by modelling.

The modelling of the 35 J-CAEI is the least accurate, because the out-of-plane displacement is overestimated and the failure stress is overestimated of about 30%, which is not the case for 10 J and 20 J-CAEI. Of course the more damage there is, the less the model is able to take into account the zone strongly damaged under the impactor. It shows clearly the limitations of the finite element models, and other approach, such as SPH or iso-parametric formulations... [40–43], could be more adapted to this type of highly damaged zone.

6.3. CAEI failure scenario

In order to evaluate and to model compression strength after edge impact, it is crucial to understand the final failure damage scenario of the specimen. In [15], the hypothesis that the fast crack propagation (normal to the loading direction at the impact point) is caused by 0° fibre compression failure was made. Then it is assumed that fibre failure in compression plays a major role in the mechanisms that drive the laminate residual strength. Let's challenge this hypothesis thanks to the CAEI model.
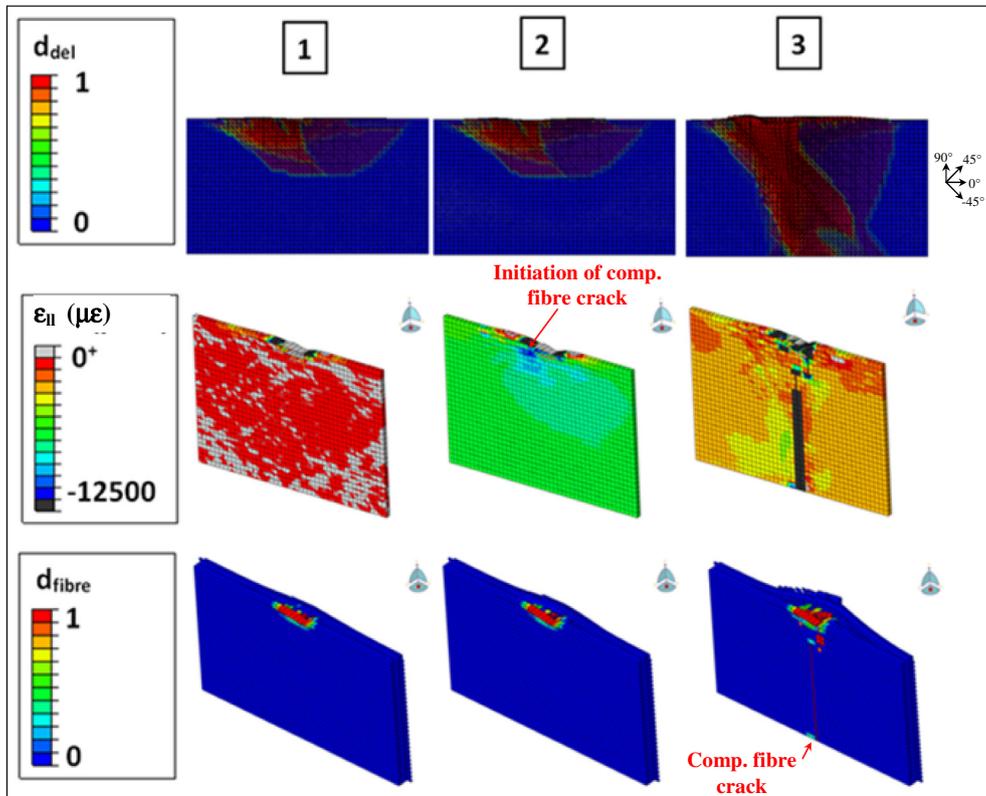

Fig. 13. Evolution of the delaminated surface, longitudinal strain and fibre failure of the 5th ply at 0° of stacking A impacted at 10 J during the CAEI test (the points 1, 2 and 3 are defined Fig. 13a).

In the model, it is possible to access to the specimen internal damage during the CAEI. The damage state, the longitudinal strain and the fibre failure are studied to enhance the damage scenario.

First of all, the delamination does not evolve a lot during the CAEI. It propagates quickly when the specimen breaks (Fig. 10a). In Fig. 13, d_{del} denotes the delamination damage (0 for undamaged and 1 for damaged), d_{fibre} the fibre damage and ε_{ll} the strain in the longitudinal (or fibre) direction. It can also be noted that $-12,500$ $\mu\varepsilon$ corresponds to the failure compression strain of the T700/M21.

Thus, focusing on the 0° ply under the impact point at the mid-thickness (ply n°5 of stacking A [90_2, -45_2, 0_4, 45_2, $\underline{\mathbf{0_2}}$]$_s$) the compressive failure strain is reached just before final failure (ε_{ll}; Fig. 13) in the area damaged by the edge impact. Finally, the final failure (d_{fibre}; Fig. 13) is driven by the compressive failure strain of the 0° ply. This seems to confirm the hypothesis of the propagation of a compressive fibre failure during the CAEI experiment.

It is interesting to note short crack propagation just before final failure (point 2, Fig. 10a). This propagation is not observed during the experiment, but future investigations are necessary to validate this. This crack being in the mid-thickness ply, it is difficult to observe it during experiment.

In order to confirm the failure scenario of propagation of compressive fibre failure numerically obtained, the evolution of out-of-plane displacement, dissipated energy in the 5th ply at 0° and global stress are plotted versus time (Fig. 14). The dissipated energy in the 5th ply corresponds to energy dissipated in the fibre failure and denotes the fibre failure developing in the ply. The 3 steps of the calculation are reported (Fig. 14a); the first step corresponding to impact, the second step corresponding to stabilization and the third step corresponding to CAI. The out-of-plane displacement increases strongly during impact loading, decreases during impact unloading, is stable during stabilization, increases progressively during the CAI and finally increases suddenly at final failure. The dissipated energy in the 5th ply is of course strictly increasing. It increases strongly during impact loading, increases a little during impact unloading, is stable during stabilization and finally increases suddenly at final failure. The stress is of course null during impact and stabilization and increases only during CAI and drops at final failure. Moreover it can be also noticed a continued and low increase of this dissipated energy early during the CAI test. If one zooms on final failure (Fig 17b), it is clear that final failure, and in particular the stress drop, is due to fibre failure and that the rise of out-of-plane displacement is only a consequence of the failure, and not the reason. The major role of the compressive fibre failure, compared to swelling or buckling, is clearly shown during CAEI, but of course the relevance of this conclusion can depend on the relevance of the model and additional experimental investigations are necessary to highlight this phenomenon.

6.4. Edge impact damage tolerance discussion

Comparison of the residual failure stress for the two stacking sequences and each impact energy level is plotted to synthesize the edge impact residual strength (Fig. 15). Residual failure stresses of the undamaged specimens are not represented because the undamaged specimens have failed earlier than expected because of peening. The modelling of stacking B is in relatively bad agreement with the experiment whatever the impact energy level (between 20% and 60% of variation). On the contrary, stacking A model, even if it presents a variation of 30% for 35 J impact energy level, is in good agreement with the experiment for the impacts at 10 J and 20 J (5% and 10% of variation). The effect of the impact energy model on the residual strength, for both stacking
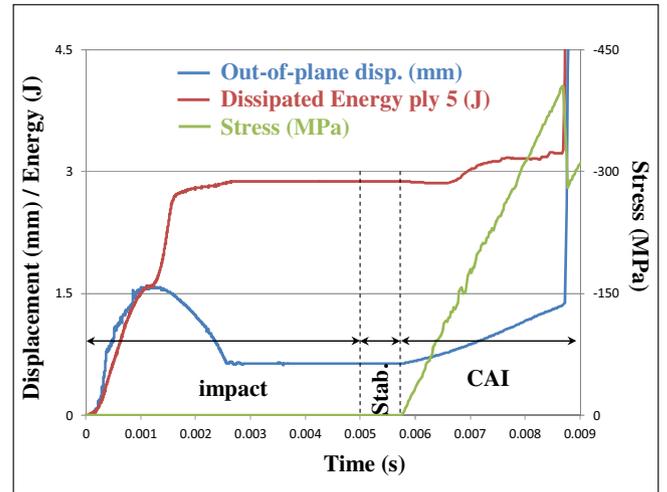
-a-
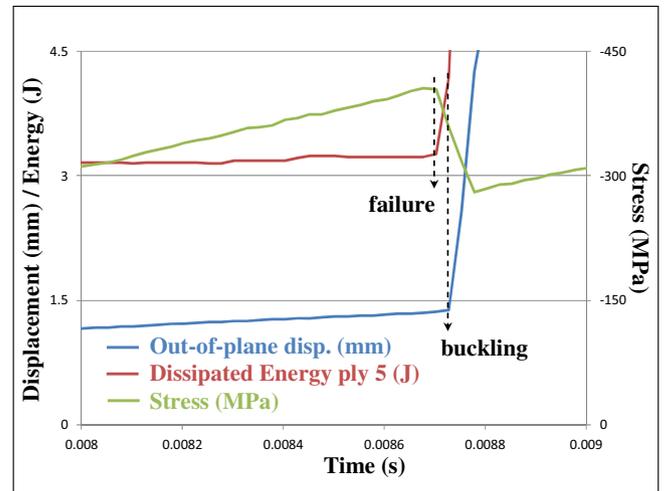
-b-

Fig. 14. Evolution of out-of-plane, dissipated energy in the 5th ply at 0° and global stress during the 3 phases of the calculation for (a) stacking A impacted at 10 J and (b) zoom on final failure.

sequences, is in a relatively good agreement (20%) with the residual strength observed during the experiment.

The model captures also the permanent indentation (Fig. 16a) and the maximum crack length (Fig. 16b) left after impact. These 2 parameters that are permanent indentation and crack length are important because they are used in the impact damage tolerance concept [1–4]. The residual stress is classically plotted versus these 2 detectability parameters in order to consider, in the same graph, the loss of characteristics due to impact and the impact detectability. Finally a relatively good correlation is found between experiment and model regarding the important number of phenomenon which is taken into account: permanent indentation after impact, force–displacement impact curve, crack length after impact, delamination after impact, stress-displacement CAEI curve, stress-out-of-plane displacement curve, CAEI final failure. Moreover it cannot be forgotten that only 14 parameters are needed to feed this model, which are all obtained using standard tests and have physical relevance (Table 1). This concept is important because it allows to consider simulating similar tests with other materials without performing complex and special identifications tests but only taking physical parameters of standard tests.
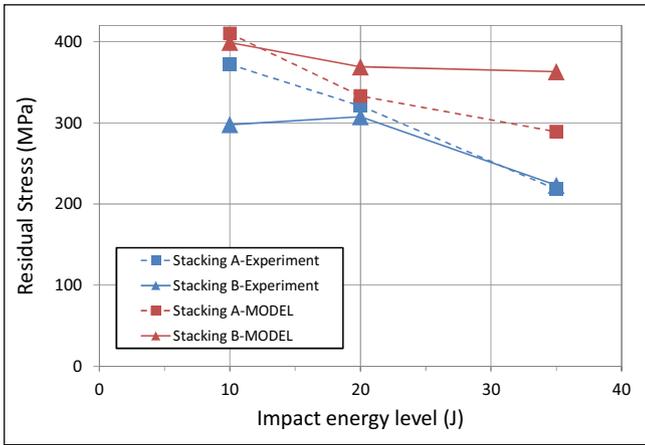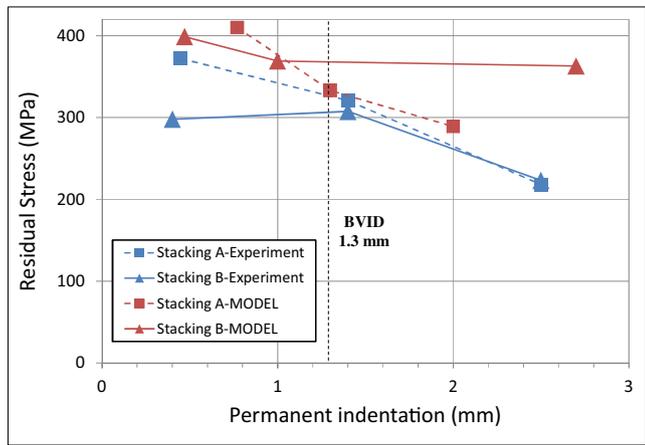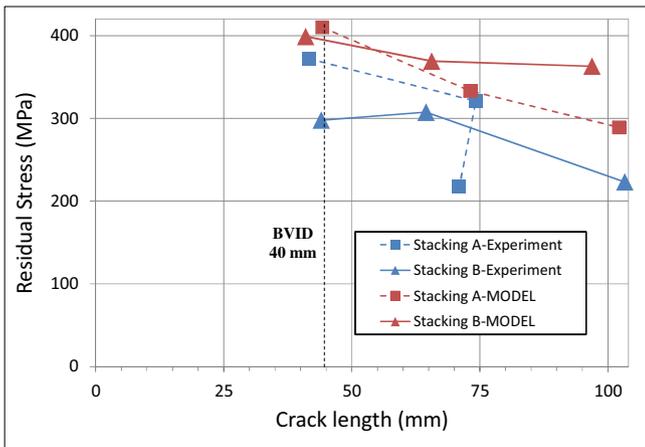
Fig. 15. Experiment/model comparison of the residual stress versus the impact energy level.

-a-

-b-

Fig. 16. Experiment/model comparison of the residual stress versus permanent indentation (a) and crack length (b).

7. Conclusion

A unique model based on DPM allows to simulate edge impact and CAEI of two highly oriented stacking sequences (A and B), representative of a real aeronautical stiffener structure. The main

conclusions of the CAEI experimental and numerical study are as follows:

All the CAEI experiments [28] show a fast crack propagation normal to the compression loading direction at the impact point. It seems that this crack is due to 0° plies' fibre failure in compression (in the loading direction). This hypothesis may be confirmed by looking at the internal damages developing in CAEI thanks to numerical model (delamination, longitudinal strain and fibre failure). Compressive fibre failure propagation plays a major role in the mechanisms that drive the laminate residual strength (Figs. 13 and 14).

Experiment/Model comparison of damage tolerance shows that the model captures relatively well the residual properties of the experiment (Figs. 15 and 16). In particular, the model seems to adequately restore the fibre failure and the matrix cracks of the experimental specimen's outside surface obtained after failure. The CAEI numerical model restores well the force versus imposed displacement during the experiment (in particular for stacking A) for impact energy levels of 10 J and 20 J. But a bad experiment/model correlation for the 35 J impact energy level proves that a phenomenon is not taken into account accurately (Fig. 11c).

For both stacking sequences, a progressive force rising is observed, then a maximum force is reached and finally the force drops sharply, experimentally as well as numerically. The correlation is not as good for 35 J tests (for stacking A or B) where some non-linearity is experimentally obtained just before the final failure; which is not numerically obtained.

Finally a relatively good correlation is found between experiment and model regarding the important number of phenomenon which are taken into account: permanent indentation after impact, force–displacement impact curve, crack length after impact, delamination after impact, stress-displacement CAEI curve, stress-out-of-plane displacement curve, CAEI final failure. Moreover it cannot be forgotten that only 14 parameters are needed to feed this model, and all are obtained using standard tests and have physical relevance (Table 1). This concept is important because it allows to consider to simulate similar tests with other materials without performing complex and special identification tests but only using physical parameters of standard tests.

To conclude, this study proposes a new method that can be used for the design and optimization of composite structures under edge impact.

Acknowledgement

References

[1] Abrate S. Impact on Composite Structures. Cambridge Press University; 1998.
[2] Rouchon J. Fatigue and damage tolerance aspects for composite aircraft structures. In: Proceedings of ICAF symposium, Delft.
[3] Hull D, Shi YB. Damage mechanism characterization in composite damage tolerance investigations. Compos Struct 1993;23(2):99–120.
[4] Bouvet C, Rivallant S. Dynamic deformation, damage and fracture in composite materials and structures, chapter 4: damage tolerance of composite structures under low-velocity impact. Silberschmidt V.: Woodhead Publishing, Elsevier; 2016.
[5] Breen C, Guild F, Pavier M. Impact damage to thick carbon fibre reinforced plastic composite laminates. J Mater Sci 2006;41:6718–24.
[6] Malhotra A, Guild FJ, Pavier M. Edge impact to composite laminates-experiments and simulations. J Mater Sci 2008;43(20):6661–7.
[7] Anderson MS, Kennedy D. Transverse shear deformation in exact buckling and vibration of composite plate assemblies. AIAA J 1993;31(10):1963–5.

[8] Anderson MS, Williams FW, Wright C. Buckling and vibration of any prismatic assembly of shear and compression loaded anisotropic plates with an arbitrary supporting structure. Int J Mech Sci 1982;25(8):585–96.

[9] Esrail F, Kassapoglou C. An efficient approach to determine compression after impact strength of quasi-isotropic composite laminates. Compos Sci Technol 2014;98:28–35.

[10] Greenhalgh E, Meeks C, Clarke A, Thatcher J. The effect of defects on the performance of post-buckled CFRP stringer-stiffened panels. Compos A Appl Sci Manuf 2003;34(7):623–33.

[11] Nyman T, Bredberg A, Schon J. Equivalent damage and residual strength for impact damaged composite structures. J Reinf Plast Compos 2000;19 (6):428–48.

[12] Rhead AT, Marchant D, Butler R. Compressive strength of composite laminates following free edge impact. Compos A Appl Sci Manuf 2010;41(9):1056–65.

[13] Rhead AT, Butler R, Baker N. Analysis and compression testing of laminates optimised for damage tolerance. Appl Compos Mater 2010;18(1):85–100.

[14] Soutis C, Smith FC, Matthews FL. Predicting the compressive engineering performance of carbon fibre-reinforced plastics. Compos A Appl Sci Manuf 2000;31:531–6.

[15] Rivallant S, Bouvet C, Hongkarnjanakul N. Failure analysis of CFRP laminates subjected to compression after impact: FE simulation using discrete interface elements. Compos A Appl Sci Manuf 2013;55:83–93.

[16] Chen P, Shen Z, Wang JY. A new method for compression after impact strength prediction of composite laminates. J Compos Mater 2002;36(5):589–610.

[17] Li N, Chen PH. Experimental investigation on edge impact damage and compression-after-impact behavior of stiffened composite panels. Compos Struct 2016;138:134–50.

[18] Suemasu H, Sasaki W, Ishikawa T, Aoki Y. A numerical study on compressive behavior of composite plates with multiple circular delaminations considering delamination propagation. Compos Sci Technol 2008;68(12):2562–7.

[19] González EV, Maimí P, Camanho PP, Turon A, Mayugo J. Simulation of drop-weight impact and compression after impact tests on composite laminates. Compos Struct 2012;94:3364–78.

[20] Tan W, Falzon BG, Chiu LNS, Price M. Predicting low velocity impact damage and Compression-After-Impact behaviour of composite laminates. Compos A Appl Sci Manuf 2015;71:212–26.

[21] Ostré B, Bouvet C, Minot C, Aboissière J. Edge impact modeling on stiffened composite structures. Compos Struct 2015;126:314–28.

[22] Choi HY, Chang K. A model for predicting damage in graphite-epoxy laminated composites resulting from low-velocity point impact. J Compos Mater 1992;26 (14):2134–69.

[23] Sun XC, Wisnom MR, Halett SR. Interaction of inter- and intralaminar damage in scaled quasi-static indentation tests: Part 2-Numerical simulation. Compos Struct 2016;136:727–42.

[24] Israr HA, Rivallant S, Bouvet C, Barrau JJ. Finite element simulation of 0°/90° CFRP laminated plates subjected to crushing using a free-face-crushing concept. Compos Part A: Appl Sci Manuf 2014;62:16–25.

[25] Hwang SF, Huang SM. Postbuckling behavior of composite laminates with two delaminations under uniaxial compression. Compos Struct 2005;68 (2):157–65.

[26] De Moura MFSF, Goncalves JPM, Marques AT, De Castro P. Modeling compression failure after low velocity impact on laminated composites using interface elements. J Compos Mater 1997;31(15):1462–79.

[27] Sebaey Abdella TAA. Characterization and optimization of dispersed composite laminates for damage resistant aeronautical structures [Ph.D. thesis]. University of Girona; 2012.

[28] Ostré B, Bouvet C, Minot C, Aboissière J. Experimental analysis of CFRP laminates subjected to compression after edge impact. Compos Struct 2016;152:767–78.

[29] Whitney J, Nuismer R. Stress fracture criteria for laminated composites containing stress concentrations. J Compos Mater 1974;8:253–65.

[30] Bouvet C, Rivallant S, Barrau JJ. Low velocity impact modeling in composite laminates capturing permanent indentation. Compos Sci Technol 2012;72 (16):1977–88.

[31] Ostré B, Bouvet C, Lachaud F, Minot C, Aboissiere J. Edge impact damage scenario on stiffened composite structure. J Compos Mater 2014;49 (13):1599–612.

[32] AITM1-0010 Airbus Test Method. Fibre reinforced plastics: determination of compression strength after impact; 2005.

[33] BSS-7260 Boeing Specification Support Standard. Advanced composite compression tests; 1998.

[34] Wisnom MR. The role of delamination in failure of fibre-reinforced composites. Philos Trans R Soc 2012;370:1850–70.

[35] Lemaitre J, Chaboche JL. Mechanics of solid materials. Cambridge University Press; 1990.

[36] Pinho ST, Robinson P, Iannucci L. Fracture toughness of the tensile and compressive fibre failure modes in laminated composites. Compos Sci Technol 2006;66(13):2069–79.

[37] Raimondo L, Iannucci L, Robinson P, Curtis PT. A progressive failure model for mesh-size-independent FE analysis of composite laminates subject to low-velocity impact damage. Compos Sci Technol 2012;72:624–32.

[38] Bazant ZP, Oh BH. Progressive crack and band theory for fracture of concrete. Mater Struct 1983;16:155–77.

[39] Israr HA, Rivallant S, Barrau JJ. Experimental investigation on mean crushing stress characterization of carbon–epoxy plies under compressive crushing mode. Compos Struct 2013;96:357–64.

[40] Jiang H, Chorzepa MG. Aircraft impact analysis of nuclear safety-related concrete structures: a review. Eng Fail Anal 2014;46:118–33.

[41] Anghileri M, Castelleti LM, Francesconi E, Milanese A, Pittofrati M. Rigid body water impact-experimental tests and numerical simulations using the SPH method. Int J Impact Eng 2011;38(4):141–51.

[42] Calamz M, Limido J, Nouari M, Espinosa C. Toward a better understanding of tool wear effect through a comparison between experiments and SPH numerical modelling of machining hard materials. Int J Refract Metal Hard Mater 2008;3:595–604.

[43] Kim JH, Paulino GH. The interaction integral for fracture of orthotropic functionally graded materials: evaluation of stress intensity factors. Int J Solids Struct 2003;40:3967–4001.